Key Points:
- We provide a three-dimensional model of Pluto's plasma environment during the New Horizons encounter
- Pluto's flat pickup tail is shaped by the significant asymmetries induced by large ion gyroradii
- A strong interplanetary magnetic field is required to explain New Horizons plasma data

Correspondence to:
M. Feyerabend,
m.feyerabend@tu-bs.de

A Three-Dimensional Model of Pluto's Interaction With the Solar Wind During the New Horizons Encounter

Moritz Feyerabend[1,2] [ID], **Lucas Liuzzo[2]** [ID], **Sven Simon[2]** [ID], and **Uwe Motschmann[1,3]** [ID]

[1]Institut für Theoretische Physik, Technische Universität Braunschweig, Braunschweig, Germany, [2]School of Earth and Atmospheric Sciences, Georgia Institute of Technology, Atlanta, GA, USA, [3]Institute for Planetary Research, German Aerospace Center, Berlin, Germany

Abstract We apply a hybrid (kinetic ions and fluid electrons) simulation model to study Pluto's plasma environment during the New Horizons encounter on 14 July 2015. We show that Pluto's plasma interaction is dominated by significant north-south asymmetries, driven by large pickup ion gyroradii on the order of 200 Pluto radii. The transition region from the ambient solar wind to the population of plutogenic ions (called the "Plutopause") also shows considerable asymmetries that cannot be explained by a fluid picture. Since the New Horizons spacecraft does not carry a magnetometer, we use our model to estimate the strength and direction of the interplanetary magnetic field (IMF) at the time of the flyby by comparing output from the hybrid simulation to the plasma signatures observed during the New Horizons encounter. We find that an IMF strength of at least 0.24 nT is required to generate the observed plasma signatures. An IMF orientation either parallel or antiparallel to Pluto's orbital motion is able to explain the observed plasma densities and velocities along the New Horizons trajectory. Our simulations are able to quantitatively reproduce all key features of the plasma observations, specifically the gradual slowing of the solar wind, as well as the location and thickness of the Plutopause and bow shock.

1. Introduction

The New Horizons (NH) flyby past the dwarf planet Pluto (radius $R_P = 1,184$ km) occurred on 14 July 2015. This encounter provided the first opportunity to collect in situ data of Pluto's atmosphere and its interaction with the dilute, weakly magnetized solar wind plasma at its orbital distance of 33 AU. On its way to the outer regions of the solar system, the NH spacecraft passed Pluto at a radial distance of 11.54 R_P on the dawnside of the dwarf planet, subsequently moving toward the downstream region where it crossed the Sun-Pluto line at a distance of ∼44 R_P (Bagenal et al., 2016). The trajectory of the flyby was slightly inclined northward against Pluto's orbital plane by approximately 3°. This caused the spacecraft to be located approximately 2 R_P south of Pluto at the time of closest approach. Radio occulation measurements by New Horizons showed that Pluto's atmosphere is dominated by N_2 but also includes CH_4 as a minor constituent (0.25%) and traces of other hydrocarbons (e.g., C_2H_4, Gladstone et al., 2016; Stern et al., 2015). The upper atmosphere was found to have a lower temperature than anticipated from preencounter models (only ∼70 K compared to the expected ∼100 K) (Gladstone et al., 2016), resulting in much lower neutral escape rates than previously calculated (10^{25} s^{-1} compared to 10^{27} s^{-1} for CH_4, and 10^{23} s^{-1} compared to 10^{27} s^{-1} for N_2, see Gladstone et al. (2016)). These authors thus concluded CH_4 to be the dominant escaping species at Pluto, instead of the previously believed N_2 (e.g., Elliot et al., 1989; Young et al., 1997, 2001). Additionally, New Horizons found Pluto's largest moon Charon to be devoid of any significant atmosphere (Gladstone et al., 2016; Stern et al., 2015). This implies that the solar wind is mass loaded by Pluto alone.

Since New Horizons does not carry a magnetometer, measurements of Pluto's plasma interaction with the solar wind were limited to particle instruments. An initial analysis of these measurements by Bagenal et al. (2016) revealed that at the time of the encounter, Pluto was exposed to a nearly homogeneous solar wind flow with an unusually high ram pressure of 6.0 pPa, compared to typical pressures of 1.7 pPa at Pluto's heliocentric distance. The increased solar wind pressure was associated with a traveling interplanetary shock that NH had detected 5 days earlier. As a result, Pluto's solar wind interaction region was much smaller than predicted by preflyby studies: Bagenal et al. (2016) estimated that at a distance of 6 R_P upstream of Pluto, the solar wind had

lost only 20% of its initial velocity. The observations also suggested that at Pluto's wakeside, the interaction region extended more than 400 R_P toward downstream. By using the maximum magnetic field observed by Voyager 2 at Pluto's heliocentric distance ($|\mathbf{B}| = 0.3$ nT), Bagenal et al. (2016) found the gyroradius of picked up CH_4^+ ions from Pluto's ionosphere to be on the order of $r_g = 190\ R_P$. This implies that Pluto's interaction should be significantly shaped by asymmetries due to ion gyration effects.

McComas et al. (2016) applied the method by Ebert et al. (2010) to analyze data from the SWAP (Solar Wind Around Pluto) instrument (McComas et al., 2008) and identified regions near Pluto dominated by either heavy plutogenic ions or light solar wind ions. These authors found that during the encounter, Pluto's solar wind interaction region was even smaller than proposed by Bagenal et al. (2016), with the region where the solar wind was slowed by 20% from the background speed value located only 4.5 R_P upstream. McComas et al. (2016) identified a narrow bow shock upstream of Pluto, possessing a thickness of only 2 ion inertial lengths, as well as a boundary layer (called the "Plutopause") that separates the solar wind ions from plutogenic heavy ions. Consistent with the large gyroradii of the pickup ions, McComas et al. (2016) identified considerable asymmetries in the structure of Pluto's heavy ion tail: At the time of the NH flyby there were significantly more heavy ions in the southern segment of the trajectory than in the northern part, due to conservation of momentum of the pickup ion population. These authors also suggested that the bow shock and Plutopause seen near Pluto are similar to the structures generated by the solar wind's interaction with comets, Mars, and Venus. Further analysis of SWAP data suggested that at the time of the NH encounter, Pluto was exposed to an outward sector of the interplanetary magnetic field, that is, the field was oriented antiparallel to Pluto's orbital motion (McComas et al., 2016; Zirnstein et al., 2016).

Because the pickup ion gyroradii are on the order of ~190 R_P (Bagenal et al., 2016), a kinetic description of the ion species near Pluto is *mandatory* to accurately describe the asymmetries in Pluto's plasma interaction. However, by comparing simulation output from a 2-D bi-ion fluid model (Sauer et al., 1997) and a 3-D multi-fluid model (Harnett et al., 2005) with hybrid simulation data, it was shown that a multifluid approach may also be able to roughly reproduce the large-scale features of Pluto's plasma interaction. Based on preencounter estimates of Pluto's atmosphere and the solar wind parameters, Delamere and Bagenal (2004) applied a hybrid simulation model to show that the interaction of the solar wind with Pluto's ionosphere generates a highly asymmetric bow shock upstream of the dwarf planet and a structured wake downstream. The interaction also generates a channel of solar wind protons that are deflected around Pluto. In a subsequent study, Delamere (2009) used a hybrid model to investigate the structure of Pluto's interaction region for a variety of possible atmospheric escape rates. That study demonstrated that for escape rates on the order of $Q_0 = 2 \cdot 10^{26}$ s^{-1}, the interaction region is bounded by a Mach cone, similar to the structures that appear at weak comets (Bagdonat & Motschmann, 2002). When increasing the escape rate by 2 orders of magnitude (to $Q_0 = 2 \cdot 10^{28}$ s^{-1}), this cone evolves into a fully detached bow shock. Delamere (2009) also showed that the flow shear between solar wind protons and heavy plutogenic pickup ions leads to the formation of bi-ion waves and may excite Kelvin-Helmholtz instabilities at the interface between the two plasma regimes (i.e., at the Plutopause).

However, these earlier studies used preencounter estimates of the solar wind parameters at 33 AU and parameters of Pluto's atmosphere that were obtained from remote telescope observations (e.g., Young et al., 1997, 2001) of the dwarf planet. Due to the enhanced solar wind pressure and the more compact state of its atmosphere, Pluto's interaction with the solar wind at the time of the flyby took place in a different region of parameter space that has not been considered by any study so far. In order to fill this gap, we implement the recent in situ observations of the solar wind (Bagenal et al., 2016) and Pluto's atmosphere (Gladstone et al., 2016) into a hybrid model to study Pluto's plasma interaction at the time of the New Horizons encounter. We investigate the influence that the large ion gyroradii have on the three-dimensional structure of Pluto's induced magnetosphere. In particular, we aim to constrain the unknown strength and orientation of the interplanetary magnetic field (IMF) at the time of the encounter by treating the upstream magnetic field strength and orientation as free parameters within the simulations. The modeled results are compared against New Horizons particle data to constrain the magnitude and orientation of the IMF during the New Horizons encounter.

Throughout this study, we use a Pluto-centered, Cartesian coordinate system, where the x axis is aligned with the Sun-Pluto line, the y axis points in the direction of Pluto's orbital motion, and the z axis points northward, completing the right-handed coordinate system. Unit vectors along the x, y, and z axes are denoted $\hat{\mathbf{x}}$, $\hat{\mathbf{y}}$, and $\hat{\mathbf{z}}$, respectively.

Table 1
Parameters of Pluto's Atmosphere Used for the Hybrid Model

Species	n_1 (m^{-3})	H_1 (km)	R_1 (R_P)	n_2 (m^{-3})	H_2 (km)	R_2 (R_P)	n_3 (m^{-3})	H_3 (km)	R_3 (R_P)
N_2	10^{20}	82.4	1	10^{16}	54.7	1.5	10^{13}	318.5	2
CH_4	10^{18}	88.3	1	10^{13}	161.5	1.5	10^{12}	509.4	2

Note. Each species is approximated by a sum of three ($i = 1, 2, 3$) barometric laws, where R_i is the reference altitude for the respective summand, n_i the number density of that species at that altitude, and H_i the scale height of the species. The parameters represent a fit to the density profiles in Figure 3 of Gladstone et al. (2016).
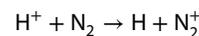
2. Model Description

We use the hybrid simulation code A.I.K.E.F. (Müller et al., 2011) in our study which treats ions as particles and electrons as a massless, charge-neutralizing fluid. This model has already been applied to analyze the plasma interaction of many unmagnetized solar system bodies, most recently Titan (Feyerabend et al., 2015, 2016), Callisto (Liuzzo et al., 2016, 2017), and Enceladus (Kriegel et al., 2014). A detailed description of the model can be found in these preceeding publications.

To describe Pluto's atmosphere, we have fitted the number density profiles of N_2 and CH_4 given in Figure 3 of Gladstone et al. (2016) with a superposition of barometric laws
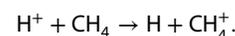
$$n_s(r) = \sum_{i=1}^{3} n_i e^{((r-R_i)/H_i)} \tag{1}$$

for each species. The reference density, scale height, and reference altitude of each summand are given by n_i, H_i, and R_i respectively; that is, for each species there are nine parameters available to fit this expression to the observations. The parameter $r = \sqrt{x^2 + y^2 + z^2}$ denotes the radial distance from Pluto's center. The fit parameters used for each species are summarized in Table 1.

Two mechanisms of ionization dominate ionospheric production at Pluto: photoionization and charge exchange (Delamere, 2009). In our model, the former is represented using the wavelength-dependent solar EUV flux model for aeronomic calculations (Richards et al., 1994), similar to Feyerabend et al. (2015). The latter is included via charge exchange between the incoming solar wind protons and plutogenic neutrals. During the New Horizons encounter, the spacecraft detected an enhanced mass flux of incoming solar wind ions (about 4 times higher, Bagenal et al., 2016). This results in the charge exchange process being even more important for the generation of Pluto's ionosphere than under average solar wind conditions, where it contributes about 50% to the mass loading (Delamere, 2009). This is considered by our model in including the ion-neutral reactions

$$H^+ + N_2 \rightarrow H + N_2^+$$

and

$$H^+ + CH_4 \rightarrow H + CH_4^+.$$

The cross sections for these reactions depend on the kinetic energy of the solar wind protons and are taken from Nakai et al. (1987). Further details about the numerical implementation of photoionization and charge exchange in the A.I.K.E.F. hybrid model can be found in Feyerabend et al. (2015), Liuzzo et al. (2015), and Kriegel et al. (2014).

We compare our simulation output with New Horizons particle measurements published in McComas et al. (2016). Table 1 in that work lists the observed solar wind velocity at eight discrete positions along the New Horizons trajectory over a range of nearly 200 R_P. The first five of these positions are located at the dawnside flank of the induced magnetosphere with distances to Pluto below 20 R_P. The last three data points are located at distances greater than 100 R_P downstream of Pluto. Due to the remote location of these three measurements, we have excluded them from our model-data comparison. To adequately resolve the physical processes that occur much closer to Pluto, we choose a simulation domain with an extension of $-20\,R_P \leq x \leq 50\,R_P$, $-20\,R_P \leq y \leq 20\,R_P$, $-12\,R_P \leq z \leq 28\,R_P$.

The grid resolution in all simulation runs is 145 km ($\approx 1/8\,R_P$) in each direction, which is comparable to the scale heights in our atmosphere model (see Table 1) and in NH data (see Figure 3 of Gladstone et al. (2016)).

The ion inertial length of the upstream solar wind protons in all runs is $x_0 = 1439$ km ($\approx 1.2 \, R_P$), while the proton gyroradius is in the range of $12-44 \, R_P$, depending on the magnetic field strength used in the model. The minimum of the proton inertial length in all runs was 200 km near the ionospheric density maximum. In this region (located near $1 \, R_P$ altitude) the ion gyroradius can locally become smaller than the grid resolution of 145 km due to the magnetic pileup and near-zero ion velocities. This is a common effect known from modeling the plasma environment of other unmagnetized bodies in the solar system (e.g., Bößwetter et al., 2004; Simon et al., 2007). However, since this layer of reduced ion gyroradii is very narrow compared to the extension of Pluto's ionosphere (~ 150 km compared to several R_P) and does not extend above the ionospheric production maximum, it does not affect the magnetic or plasma signatures associated with Pluto's plasma interaction (e.g., the structure and location of the bow shock).

The time step in all simulations is on the order of $10^{-3} \, \Omega_0^{-1}$, where Ω_0 is the gyrofrequency of the upstream solar wind protons. This time step is always about 2 orders of magnitude well below the smallest possible ion time scale of $\sim 10^{-1} \, \Omega_0^{-1}$ and also ensures that the Courant condition is always met in our simulation. Note that not satisfying the Courant condition at all times in our hybrid model would result in numerical instability of the simulations (Müller et al., 2011).

In all simulation runs we use a threshold of 5 particles-per-cell (ppc) for the solar wind protons and 20 ppc for each Plutogenic heavy ion species. To ensure that enough particles are present in each cell at all times, a splitting and merging method is used for the macroparticles: If the number of macroparticles for a certain species in a given cell is less than this threshold, particles of the species are split into two until the threshold is reached again. The method conserves the mass, momentum, and kinetic energy of the particles in each cell and is described in detail in Müller et al. (2011).

To constrain the magnitude of the IMF during the New Horizons encounter, Pluto's plasma interaction is investigated for four different upstream magnetic field strengths: 0.08 nT, 0.16 nT, 0.24 nT, and 0.3 nT. This range of values covers the Voyager 2 observations of the magnetic field strength near 33 AU where Pluto's orbit is located. In these four simulations, the upstream magnetic field is aligned with the $-y$ axis (i.e., the IMF is antiparallel to Pluto's orbital direction). As a consequence, the pickup cycloids in those runs are mainly located in the $z > 0$ hemisphere. To substantiate the result of Zirnstein et al. (2016) and McComas et al. (2016) that an IMF directed along the $-y$ axis was indeed the most likely orientation during the encounter, we also consider a fifth simulation with a magnetic field of strength 0.3 nT, and $\mathbf{B}_0$ oriented along the $+y$ axis (i.e., parallel to Pluto's orbital direction).

In all model runs the solar wind plasma upstream of Pluto consists of H^+ protons with upstream number density $n_0 = 0.025 \, \text{cm}^{-3}$, upstream flow velocity $u_0 = 403$ km/s (directed along $+x$), and ion temperature $kT_{H^+} = 0.66$ eV (see Table 1 in Bagenal et al., 2016). The electron temperature is assumed to be $kT_e = 1$ eV. The Alfvénic and magnetosonic Mach numbers and plasma betas of the upstream solar wind in these runs range from $M_A = 9.73$, $M_{MS} = 8.93$, and $\beta_{SW} = 0.18$ for the $|\mathbf{B}_0| = 0.3$ nT case to $M_A = 36.48$, $M_{MS} = 19.2$, and $\beta_{SW} = 2.61$ for the $|\mathbf{B}_0| = 0.08$ nT case. Thus, the solar wind during the NH encounter is always highly superalfvénic and supermagnetosonic.

3. General Characteristics of Pluto's Solar Wind Interaction

A three-dimensional picture of Pluto's interaction with the solar wind for an upstream magnetic field vector of $\mathbf{B}_0 = (0, -0.24, 0)$ nT (i.e., the gyroradius of methane pickup ions is $r_g \approx 236 \, R_P$) is visible in Figure 1. Figure 1a shows the draped magnetic field lines of the IMF around the Pluto obstacle in the $z = 0$ plane, color coded with the local B_x value. Depicted in yellow is a $|\mathbf{B}| = 1.1 |\mathbf{B}_0|$ contour of the magnetic field strength, illustrating the outer edge of the parabolic bow shock that forms upstream of Pluto. Figure 1b shows a three-dimensional picture of the solar wind bulk velocity near Pluto in the $x = -5 \, R_P$, $y = 0 \, R_P$, and $z = -3 \, R_P$ planes. The black vectors also show the direction of the solar wind protons in those planes. Additionally, the white arrows represent the bulk speed and direction of the plutogenic heavy ions (CH_4^+ and N_2^+) as they are picked up by the ambient electromagnetic fields and convected away from Pluto. The asymmetries resulting from the large gyroradii of the pickup ions are clearly visible, as only a small segment of the cycloidal arcs is seen in the $y = 0$ plane. These arcs possess an extension of about $2 \, r_g \approx 472 \, R_P$ along the z axis and a width of $2\pi r_g \approx 1482 \, R_P$ in x direction.

Figure 2 shows two-dimensional cuts of Pluto's interaction region in the $z = 0$ plane, with number density and bulk velocity of the solar wind protons and CH_4^+ pickup species plotted. Additionally, the electric and magnetic
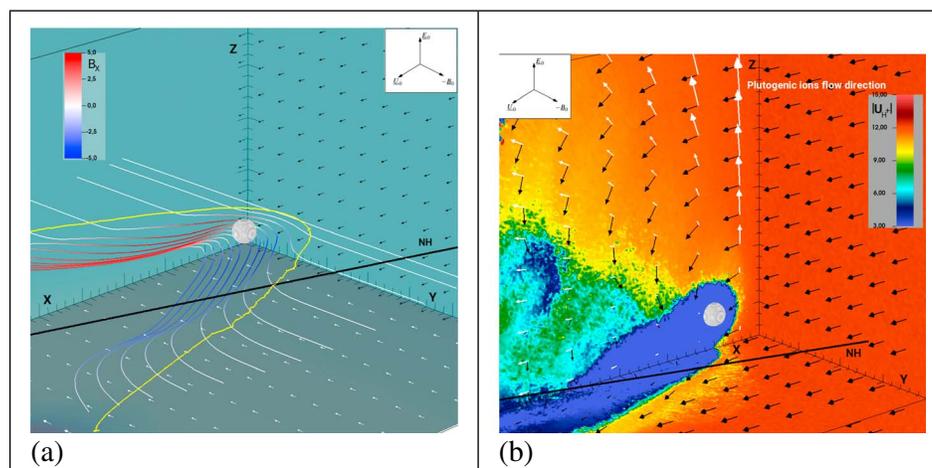
Figure 1. (a) Draped magnetic field lines near Pluto during the New Horizons encounter, color coded with the B_x value of the magnetic field. The yellow $|\mathbf{B}| = 1.1\,|\mathbf{B}_0|$ ($|\mathbf{B}_0| = 0.24$ nT) isoline of the magnetic field strength represents the outer border of the bow shock. The white arrows at the bottom plane indicate the upstream magnetic field direction. Black arrows indicate the direction of the incoming solar wind. (b) Three-slice of the solar wind bulk velocity $|\mathbf{u}_{H+}|$. Black arrows indicate the solar wind flow direction in the depicted planes. The white arrows show the flow direction of plutogenic heavy ions. New Horizons trajectory is indicated by the black line in both plots. Note that due to the perspective in these plots the solar wind flows from "right" to "left."

fields are included. We find a bow shock standoff distance of $4-5\,R_P$ upstream of Pluto, as visible in Figure 2e as well as in Figure 1a. This is consistent with the findings of McComas et al. (2016) who extrapolated the bow shock distance to be approximately $4.5\,R_P$ at Pluto's upstream side, using NH measurements of the reduced solar wind velocity near the flanks of the interaction region. This confirms that Pluto's induced magnetosphere was indeed in a rather compressed state at the time of the NH encounter, due to the enhanced dynamic pressure of the impinging solar wind. Our simulations also show an increase in the solar wind density by up to a factor of 4 at the flanks of Pluto's magnetotail (see Figures 2a and 2e), which is a result of the accumulation of solar wind particles as they encounter the shock and are decelerated and diverted around the obstacle.

In the $z = 0$ plane (i.e., perpendicular to the upstream convective electric field $\mathbf{E}_0 = -\mathbf{u}_0 \times \mathbf{B}_0$), Pluto's tail structure is highly symmetric with respect to the x axis, as can be seen in all quantities in Figure 2. In this plane (and other $z = $ const planes), the structure of Pluto's induced magnetotail is mainly governed by pressure balance: Inside of the magnetic lobe regions ($1\,R_P < |y|$, i.e., outside the magnetic neutral sheet), the magnetic pressure is enhanced compared to the ambient solar wind plasma (see Figure 2e), and the ion number densities of both solar wind and plutogenic ions are low (see Figures 2a and 2c). As can be seen from Figure 2f, the electric field is enhanced at the outer edges of the wakeside current sheet. This enhancement is mainly governed by the Hall term in the electric field equation. In planes perpendicular to $\mathbf{E}_0$, the heavy ions that originate from Pluto are mainly confined to the narrow magnetic neutral sheet between the two lobes (see Figures 2c and 2e). The formation of a narrow channel of escaping ions in planes containing the background magnetic field is typical for the plasma interaction of nonmagnetized bodies, such as weak comets (Motschmann & Kührt, 2006), Mars (Bößwetter et al., 2004), or Titan (Simon & Motschmann, 2009).

The observed Plutopause marks the transition from outside of (dominated by solar wind ions) to inside of (dominated by plutogenic heavy ions) Pluto's induced magnetosphere (McComas et al., 2016). Although the solar wind density sharply drops at the outer edges of Pluto's magnetotail (Figure 2a), the region between the outer flanks of the magnetotail and the central plasma sheet is nearly devoid of heavy ions (Figure 2c). Instead, we find that the transition between solar wind ions and plutogenic ions in planes parallel to Pluto's orbital plane ($z = 0$) depends on the altitude above or below that plane. This stratification can be seen in Figure 3, which shows a cut through the downstream magnetotail at $x = 15\,R_P$. In this plane, Pluto's magnetotail has an "onion-like" shape with a bulge near $z = 0$ that transitions into a narrow channel when moving northward into the $z > 0$ hemisphere. This shape is generated by the deflection of the solar wind around the interaction region, as visible in Figures 3a and 3c.
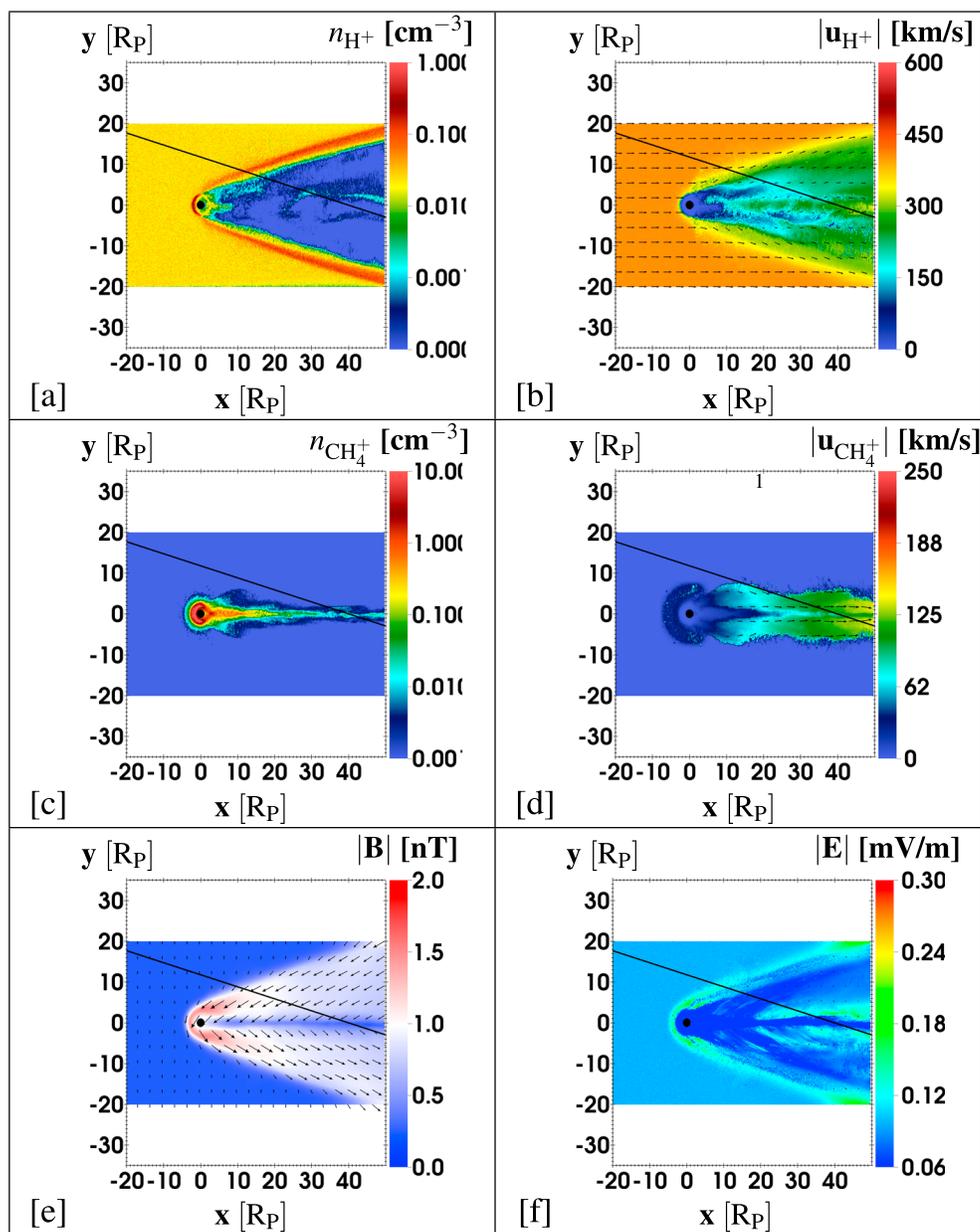
Figure 2. Plasma quantities in the $z = 0$ plane for the simulation with $|\mathbf{B}_0| = 0.24$ nT: (a) Solar wind number density n_{H^+}, (b) solar wind bulk velocity $|\mathbf{u}_{H^+}|$, (c) pickup ion number density $n_{CH_4^+}$, (d) pickup ion bulk velocity $|\mathbf{u}_{CH_4^+}|$, (e) magnetic field strength $|\mathbf{B}|$, and (f) electric field strength $|\mathbf{E}|$. The projection of New Horizons trajectory onto this plane is indicated by the black line.
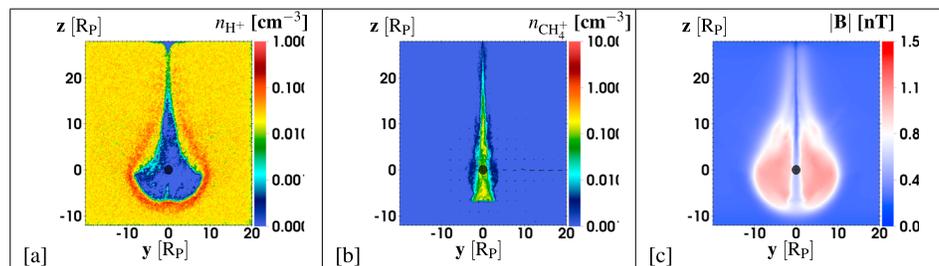

Figure 3. (a) Solar wind number density n_{H^+}, (b) pickup ion number density $n_{CH_4^+}$, and (c) magnetic field strength $|\mathbf{B}|$ in the $x = 15\ R_P$ plane downstream of Pluto.
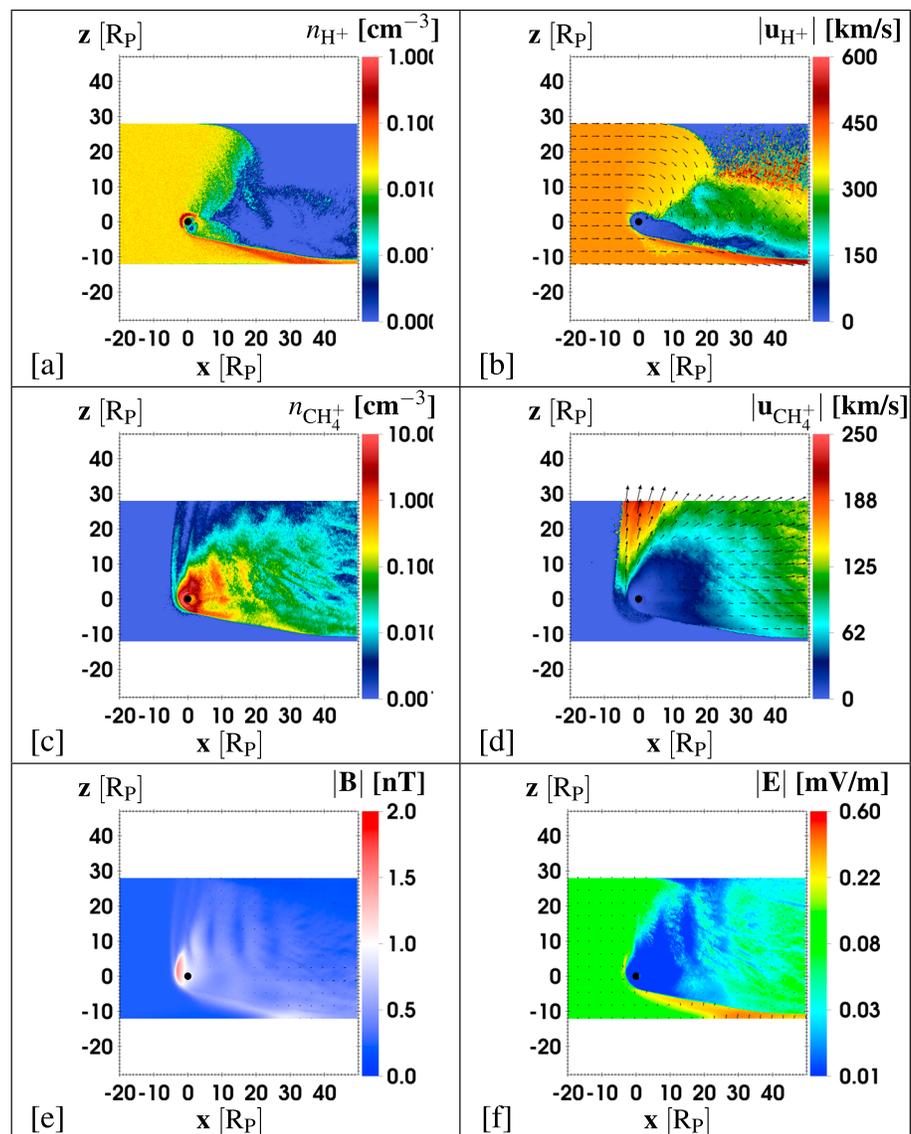
Figure 4. Plasma quantities in the $y = 0$ plane for the simulation with $|\mathbf{B}_0| = 0.24$ nT: (a) Solar wind number density n_{H^+}, (b) solar wind bulk velocity $|\mathbf{u}_{H^+}|$, (c) pickup ion number density $n_{CH_4^+}$, (d) pickup ion bulk velocity $|\mathbf{u}_{CH_4^+}|$, (e) magnetic field strength $|\mathbf{B}|$, and (f) electric field strength $|\mathbf{E}|$.

As we can see in Figures 3a and 3b, there are three distinct regions, where the transition between the solar wind and plutogenic ions is structured differently. First, in the $z < 0$ hemisphere, the heavy plutogenic ions only partially fill the "body of the onion," which leaves a volume near the outer edges of the magnetotail where the density of both solar wind and plutogenic heavy ions is very low. In this region, the magnetic pressure compensates for the reduced particle pressure of the solar wind and plutogenic ions (see Figure 3c).

Second, in the $z > 0$ hemisphere up to an altitude of $\sim 15\,R_P$, the region of depleted solar wind density near the flanks shows a low-density population of plutogenic heavy ions that connects to the outer boundary of the "onion." This transition is now defined by a more gradual decrease in the solar wind density and takes places on a scale of several Pluto radii. The third region appears at even higher altitudes above $z > 0$, where the thin pickup tail leads to a more rapid transition between the solar wind and plutogenic ions. It should be noted, however, that the locations of these three regions depend on the tailward (x) distance to Pluto, as well as on the upstream solar wind parameters.

Figure 4 shows the same quantities as Figure 2 but in the $y = 0$ plane (i.e., parallel to $\mathbf{u}_0$ and $\mathbf{E}_0$) of Pluto's interaction. The tail structure in this plane is significantly asymmetric between the northern ($z > 0$) and

southern ($z < 0$) hemisphere. Since the gyroradii of the plutogenic heavy ions are up to about 200 Pluto radii in size, their local escape trajectories are nearly parallel to the upstream convective electric field direction (i.e., they move mainly along $+\hat{z}$; see also Figures 4c and 4d). Therefore, these ions only perform a fraction of a pickup cycloid within the simulation domain. This motion of the plutogenic ions along the $+z$ direction combined with their confinement between Pluto's magnetic lobes (see Figure 3) leads to the formation of a "flat" (thickness $< 4\,R_P$) pickup tail in the plane perpendicular to $\mathbf{B}_0$, a feature also found at weak comets (Koenders et al., 2015).

In the $z > 0$ hemisphere of Pluto's interaction, the escaping plutogenic ions intermix with solar wind ions, and a clearly defined "Plutopause" layer, *is not* discernible (see Figures 4a and 4c). In this hemisphere, the solar wind is also accelerated antiparallel to the plutogenic ions (i.e., southward along $-\hat{z}$) by the local Lorentz forces (see Figure 4b). The "raining down" of solar wind ions into Pluto's southern magnetotail is also visible in Figure 1b. This effect has also been seen in simulation results for weakly outgassing comets (Bagdonat & Motschmann, 2002) and in earlier model runs for Pluto (Delamere, 2009). This motion conserves the total momentum of the plasma as the solar wind overlaps with the dense beam of northward moving pickup ions (Figure 4d). The antialignment of both plasma flows is a source for bi-ion waves, which can be seen in the wave-like patterns in Figures 4c, 4e, and 4f.

Although a Plutopause is not generated in the $z > 0$ hemisphere, two conditions favor the formation of a sharp "Plutopause" boundary in the $z < 0$ hemisphere. On the one hand, the northward pointing convective electric field prevents the slow plutogenic ions from penetrating into the solar wind. On the other hand, solar wind ions that approach this boundary from upstream experience the electric field due the mainly southward pointing pressure gradient $-\nabla P_e$, which is generated by the heavy plutogenic ions that accumulate south of Pluto's orbital plane (see Figure 3b). The resulting Plutopause in this hemisphere is therefore much thinner and more sharply defined compared to the three regions identified in Figure 3 (that can be seen in different $z = \text{const}$ planes of the "onion"), with the transition between solar wind ions and plutogenic ions occurring over only a fraction of a Pluto radius (see Figures 4a and 4c).

A similar transition layer between impinging upstream plasma and pickup ions (often called an "Ion Composition Boundary") has also been found at other solar system bodies, for example, at Mars (Sauer & Dubinin, 2000) and Titan (Wahlund et al., 2005). Using hybrid simulations, Simon et al. (2007) showed that such boundary layers can generally be expected for superalfvénic, supersonic plasma interactions of unmagnetized bodies. They also showed that the structure of these boundary layers displays significant asymmetries with respect to the direction of the convective electric field, if the ion gyroradii are comparable to the size of the obstacle. Our results therefore demonstrate that at Pluto, the "Plutopause" boundary layer has the same properties as the Ion Composition Boundaries at other solar system bodies.

Compared to the preencounter hybrid modeling results of Pluto's interaction with the solar wind by Delamere (2009), our modeled plasma interaction signatures for NH conditions are settled between their cases of an intermediate ($Q_0 = 2 \cdot 10^{27}\,\text{s}^{-1}$) and low ($Q_0 = 0.2 \cdot 10^{27}\,\text{s}^{-1}$) neutral escape rate Q_0 of molecular nitrogen N_2. Note that their model uses a comet-like neutral gas profile that decreases with $1/r^2$ (see equation (15) in Delamere, (2009)) and uses Q_0 to determine the maximum neutral density at the surface, as opposed to our atmosphere model which is based on in situ observations (see equation (1). Delamere (2009) obtained a plasma interaction of Pluto that is characterized by a nondetached bow shock (or Mach cone) and considerable asymmetries in the structure of the induced magnetotail due to the large gyroradii. The solar wind in the model of Delamere (2009) is assumed to be slightly slower ($\sim$340 km/s) and less dense (0.01 cm^{-3}) than in the New Horizons case. Unlike in their $Q_0 = 2 \cdot 10^{27}\,\text{s}^{-1}$ case, we do not see indications for the excitation of Kelvin-Helmholtz instabilities in our simulations. However, our simulation domain does not cover the regions where the instabilities were seen by Delamere (2009).

Note that the New Horizons encounter revealed the neutral escape rates to be orders of magnitude ($10^{23}\,\text{s}^{-1}$–$10^{25}\,\text{s}^{-1}$) lower than assumed by Delamere (2009). Applying these parameters to the model of Delamere (2009) would likely result in a much weaker plasma interaction than actually observed by New Horizons. The reason for this lies in the preencounter model of the neutral atmosphere used in that work, which underestimates the neutral density by up to 4 orders of magnitude compared to the actual observations. The (now known to be unrealistic) high neutral escape rates used in Delamere (2009) were able to partially counter this effect, effectively producing a similar plasma interaction as in our simulations. Compared with previous simulation models of Pluto's plasma interaction, our model is therefore the first one
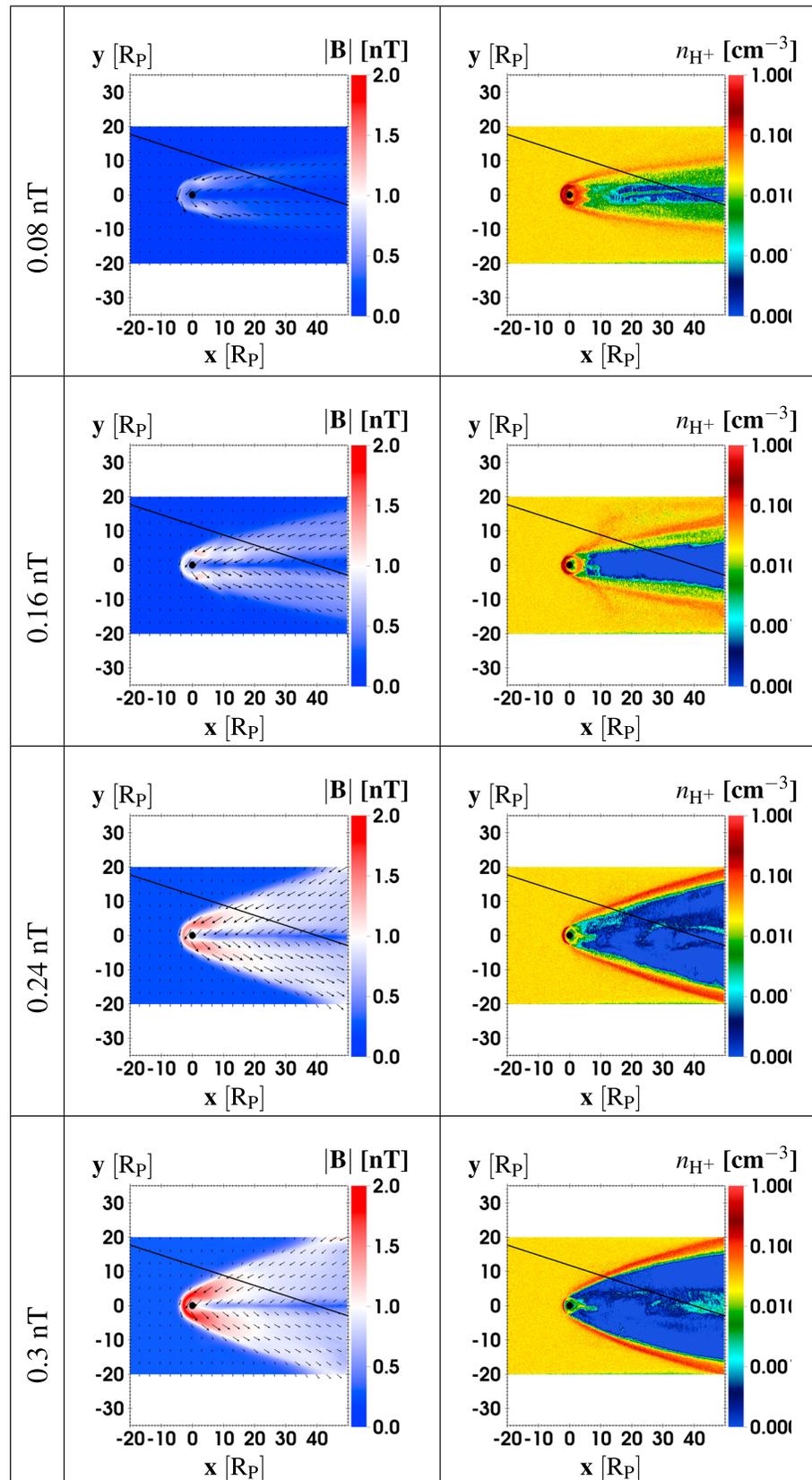
Figure 5. Comparison of the magnetic field strength $|\mathbf{B}|$ and solar wind number density n_{H^+} in the $z = 0$ plane for simulations with different IMF field strength $|\mathbf{B}_0|$ ranging from (top) 0.08 nT to (bottom) 0.3 nT.
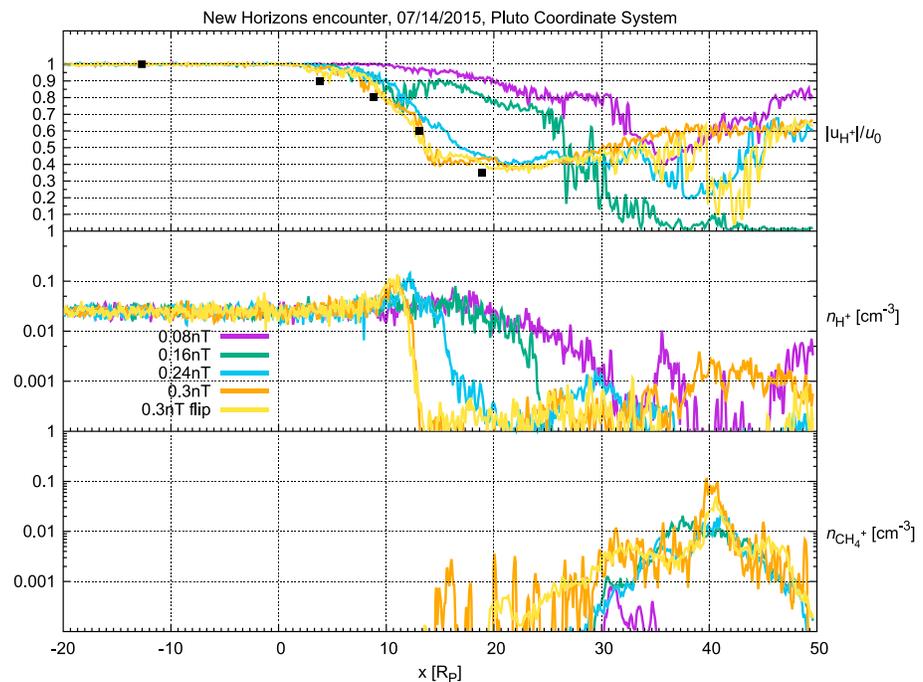
Figure 6. Hybrid model results for varying IMF strengths (colored lines) in the range of 0.08–0.3 nT along the New Horizons trajectory. (top) Normalized solar wind bulk velocity $|u_{H^+}|/u_0$. (middle) Solar wind number density n_{H^+}. (bottom) Pickup ion number density n_{H^+}. The black squares in the top panel denote observations from the New Horizons SWAP instrument, which measured the solar wind velocity near Pluto (see Table 1 of McComas et al. (2016)).

to include in situ observations of Pluto's atmosphere (which is far less extended than previously assumed), as well as realistic parameters of the upstream plasma at the time of the New Horizons flyby.

4. Constraining the IMF During the New Horizons Encounter

The model results in Figure 5 show how the structure of Pluto's induced magnetosphere changes in the $z = 0$ plane (i.e., approximately the New Horizons flyby plane), when the IMF strength is increased from 0.08 nT to 0.3 nT while all other parameters of the solar wind are kept constant (see section 2). As a result, the Alfvénic and sonic Mach numbers of the upstream plasma decrease in between these runs, causing the opening angle of the shock parabola to become wider with increasing strength of the IMF. The location of the bow shock stand-off distance is robust against changes of the IMF strength and remains approximately at 4–5 R_P upstream. This is to be expected, since the standoff distance is mainly influenced by the mass loading into the upstream solar wind (Koenders et al., 2013) (which does not change between these runs).

As visible in Figure 5, the spatial extention of the magnetic neutral region does not vary much in size as the IMF strength increases. For each simulation, this region in Pluto's wake is always approximately 2 R_P in thickness in the $z = 0$ plane. Additionally, while the solar wind number density gradually decreases by 2 orders of magnitude over multiple Pluto radii at the flanks of the tail for the $|\mathbf{B}_0| = 0.08$ nT case, this decrease becomes much sharper for the $|\mathbf{B}_0| = 0.3$ nT case. There the decrease in solar wind number density occurs over only a fraction of a Pluto radius.

Figure 6 shows the bulk velocity of the solar wind protons u_{H^+}, the solar wind number density n_{H^+} and the number density of the methane pickup ions $n_{CH_4^+}$ along the New Horizons trajectory for the different simulations in our parameter study. SWAP measurements of the solar wind velocity, as provided in Table 1 in McComas et al. (2016), are indicated by the five black squares. As we can see, an IMF field strength of at least $|\mathbf{B}_0| = 0.24$ nT (blue curve) is needed to generate any significant deceleration of the solar wind near the observed locations. The simulation with $|\mathbf{B}_0| = 0.24$ nT correctly reproduces the downward trend of the solar wind velocity from 10% slowing to the maximum observed slowing of about 65% (~140 km/s) over a tailward distance of 15 R_P (from the second to the fifth data point). However, the modeled decrease is slightly shifted toward downstream compared to the observed positions. Only simulations that use an IMF strength

of $|\mathbf{B}_0| = 0.3$ nT (yellow and orange curves) are in excellent agreement with the observed values. This supports the considerations of Bagenal et al. (2016), who also suggested the magnetic field strength during the encounter to be near the maximum of the values observed by Voyager 2.

Figure 6 shows also that simulations with an upstream magnetic field strength of $|\mathbf{B}_0| = 0.08$ nT (purple curve) or $|\mathbf{B}_0| = 0.16$ nT (green curve) cannot reproduce any deceleration of the solar wind near the observed locations. For those runs the initial decrease in solar wind velocity occurs much farther downstream compared to the other runs, in accordance with the narrower opening angle of the shock parabola at higher Mach numbers (see Figure 5).

The comparison of the modeled bulk speed with the measured data strongly suggests that the IMF strength at the time of the New Horizons encounter was at the upper edge of the range measured by Voyager 2. The modeled results of the solar wind number density (Figure 6, middle) support this idea. Based on SWAP measurements, McComas et al. (2016) showed that the solar wind ion counts significantly dropped between $x = 13.1\ R_P$ and $x = 18.9\ R_P$ (i.e., between the fourth and fifth data point). Our model results show that only runs with a high IMF strength ($|\mathbf{B}_0| \geq 0.24$ nT) produce a significant drop by 2 orders of magnitude in solar wind density near these locations, with the $|\mathbf{B}_0| = 0.24$ nT run being closest to the reported locations.

McComas et al. (2016) and Zirnstein et al. (2016) used New Horizons particle measurements to infer an IMF orientation that was antiparallel to Pluto's orbital motion (i.e., directed along the $-y$ axis) during the encounter. McComas et al. (2016) inferred this from the observation that more heavy ions were found in the $z < 0$ segment of the NH trajectory than in the $z > 0$ segment. They explained this observation via momentum conservation of the pickup ions, because for the IMF being aligned with $-\hat{\mathbf{y}}$, the pickup ions would move faster into the $\mathbf{E}_0 = -\mathbf{u}_0 \times \mathbf{B}_0$ direction (i.e., into Pluto's northern hemisphere, $z > 0$), leaving more heavy ions accumulated in the southern ($z < 0$) hemisphere. In support of this idea, we also find more plutogenic ions in the southern hemisphere compared to the northern hemisphere, which can be seen in Figure 3b. Zirnstein et al. (2016) combined information about SWAP's field of view with the energies at which SWAP detected heavy ions from an isolated burst of heavy ions to come to the same conclusion about the IMF orientation.

We also tested the other possible orientation of the IMF at Pluto's orbital distance, that is, along the $+y$ axis, with an IMF strength of $|\mathbf{B}_0| = 0.3$ nT (yellow curve in Figure 6). Reversing the orientation of the IMF produces nearly the same results in the solar wind velocity as with an orientation along $-y$ (yellow versus orange curve). The reason for this is that the flyby plane nearly coincides with the symmetry plane of the plasma interaction in both cases, (i.e., the $z = 0$ plane). In this plane asymmetries in the magnitude of the ion velocities associated with pickup ion gyration are not yet developed. For the NH trajectory, only in planes that are significantly above or below the $z = 0$ plane these asymmetries will have a visible impact that allows to distinguish between different orientations of the IMF: In the $z > 0$ hemisphere, the measured drop in solar wind velocity would have been observed at a later time during the flyby and would not have lasted as long as than in the opposite hemisphere, due to the different extensions of the magnetotail (see also Figure 3a). In these regions the density of pickup ions would also be an even better indicator of the IMF direction than their bulk velocity. For instance, if the IMF points along $-y$, in a plane far below the equatorial plane no pickup ions at all would be detected, leaving only the other possibility for the orientation of $\mathbf{B}_0$.

In conclusion, while we are not able to unambiguously determine the IMF orientation at the time of the flyby based on the solar wind velocity alone, the simulated heavy ion data support the result of Zirnstein et al. (2016) and McComas et al. (2016) who found a retrograde ($-y$) orientation of the IMF.

5. Summary and Concluding Remarks

In this study we have applied a hybrid model to analyze Pluto's interaction with the solar wind during the New Horizons encounter. We have demonstrated that an enhanced IMF strength of at least 0.24 nT is needed in order to quantitatively explain the observed decrease of the solar wind velocity in Pluto's wake at the time of the encounter. This IMF strength is consistent with the observation of an increased dynamic pressure in the solar wind during the flyby (Bagenal et al., 2016). The enhanced dynamic pressure results in a standoff distance of the bow shock that is closer to Pluto than expected, located at only $4-5\ R_P$ upstream. Both possible orientations of the IMF, either parallel or antiparallel to Pluto's orbital direction, produce results that are consistent with the observed solar wind bulk velocity. Since the New Horizons encounter took place approximately in the symmetric plane ($z = 0$) of the plasma interaction, the observed slowing of the solar wind velocity would
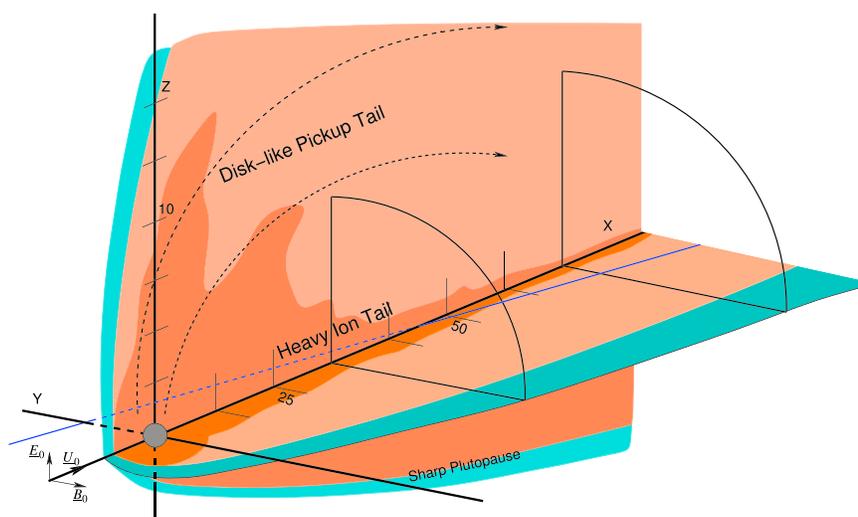
Figure 7. Sketch of Pluto's plasma interaction with the solar wind at the time of New Horizons encounter. The axes are scaled in units of Pluto radii. Orange colors indicate plutogenic heavy ions for dense (dark orange) and less dense (light orange) values. The border of the induced magnetosphere is determined by the flow diversion of solar wind ions, indicated by turquoise colors. The New Horizons trajectory is shown by the blue line. The curved dashed black lines in the pickup tail represent a small section of the large-scale pickup cycloids of the plutogenic heavy ions.

be the same for both options. However, the northward escaping heavy ions as well as the higher heavy ion content in the southern hemisphere in our simulations (see Figures 3b and 4c) support the results of Zirnstein et al. (2016) and McComas et al. (2016) who found a retrograde ($-y$) orientation of the IMF at the time of the flyby.

A schematic sketch of Pluto's interaction region (consistent with our model and in situ observations) is depicted in Figure 7. Pluto's induced magnetosphere is strongly influenced by the large pickup ion gyroradii on the order of $\sim 200\ R_P$. In the direction of the convective electric field $\mathbf{E}_0$, a flat, disk-like pickup tail of only a few Pluto radii thickness is formed. This is due to the heavy ions being mainly confined to the neutral region between the magnetic lobes which are formed by draping of the IMF around Pluto's ionosphere. The portion of the solar wind that encounters this pickup tail is diverted southward, "raining" down into Pluto's induced magnetosphere.

The transition from solar wind (turquoise colors in Figure 7) to heavy ions (orange colors in Figure 7) is also affected by the highly asymmetric interaction. A sharp transition over only a fraction of a Pluto radius, similar to an Ion Composition Boundary, is visible only in the southern ($z < 0$) hemisphere of the $y = 0$ and neighboring planes (i.e., in planes parallel to $\mathbf{E}_0$, cf. Figure 3). A more gradual transition (over several Pluto radii) can be seen in planes perpendicular to $\mathbf{E}_0$, where the increased magnetic pressure in the lobe regions separates the heavy ions from the solar wind more effectively. Though our model may create a consistent magnetic field this study is not an appeal to drop magnetometers for future space missions.

References

Bagdonat, T., & Motschmann, U. (2002). From a weak to a strong comet—3D global hybrid simulation studies. *Earth, Moon and Planets*, *90*, 305–321.

Bagenal, F., Horányi, M., McComas, D. J., McNutt, R. L., Elliott, H. A., Hill, M. E., . . . Zangari, A. M. (2016). Pluto' interaction with its space environment: Solar wind, energetic particles, and dust. *Science*, *351*, AAD9045. https://doi.org/10.1126/science.aad9045

Bößwetter, A., Bagdonat, T., Motschmann, U., & Sauer, K. (2004). Plasma boundaries at Mars: A 3-D simulation study. *Annales Geophysicae*, *22*, 4363–4379.

Delamere, P. A. (2009). Hybrid code simulations of the solar wind interaction with Pluto. *Journal of Geophysical Research*, *114*, A03220. https://doi.org/10.1029/2008JA013756

Delamere, P. A., & Bagenal, F. (2004). Pluto's kinetic interaction with the solar wind. *Geophysical Research Letters*, *31*, L04807. https://doi.org/10.1029/2003GL018122

Ebert, R. W., McComas, D. J., Rodriguez, B., Valek, P., & Weidner, S. (2010). A composition analysis tool for the Solar Wind Around Pluto (SWAP) instrument on new horizons. *Space Science Reviews*, *156*, 1–12. https://doi.org/10.1007/s11214-010-9683-6

Elliot, J. L., Dunham, E. W., Bosh, A. S., Slivan, S. M., Young, L. A., Wasserman, L. H., & Millis, R. L. (1989). Pluto's atmosphere. *Icarus*, *77*, 148–170. https://doi.org/10.1016/0019-1035(89)90014-6

Feyerabend, M., Simon, S., Motschmann, U., & Liuzzo, L. (2015). Filamented ion tail structures at titan: A hybrid simulation study. *Planetary and Space Science*, *117*, 362–376. https://doi.org/10.1016/j.pss.2015.07.008

Feyerabend, M., Simon, S., Neubauer, F. M., Motschmann, U., Bertucci, C., Edberg, N. J. T., ... Kurth, W. S. (2016). Hybrid simulation of Titan's interaction with the supersonic solar wind during Cassini's T96 flyby. *Geophysical Research Letters*, *43*, 35–42. https://doi.org/10.1002/2015GL066848

Gladstone, G. R., Stern, S. A., Ennico, K., Olkin, C. B., Weaver, H. A., Young, L. A., ... Zirnstein, E. (2016). The atmosphere of Pluto as observed by New Horizons. *Science*, *351*, AAD8866. https://doi.org/10.1126/science.aad8866

Harnett, E. M., Winglee, R. M., & Delamere, P. A. (2005). Three-dimensional multi-fluid simulations of Pluto's magnetosphere: A comparison to 3D hybrid simulations. *Geophysical Research Letters*, *32*, L19104. https://doi.org/doi:10.1029/2005GL023.178

Koenders, C., Glassmeier, K.-H., Richter, I., Motschmann, U., & Rubin, M. (2013). Revisiting cometary bow shock positions. *Planetary and Space Science*, *87*, 85–95. https://doi.org/10.1016/j.pss.2013.08.009

Koenders, C., Glassmeier, K.-H., Richter, I., Ranocha, H., & Motschmann, U. (2015). Dynamical features and spatial structures of the plasma interaction region of 67P/Churyumov-Gerasimenko and the solar wind. *Planetary and Space Science*, *105*, 101–116. https://doi.org/10.1016/j.pss.2014.11.014

Kriegel, H., Simon, S., Meier, P., Motschmann, U., Saur, J., Wennmacher, A., ... Dougherty, M. K. (2014). Ion densities and magnetic signatures of dust pick-up at Enceladus. *Journal of Geophysical Research: Space Physics*, *119*, 2740–2774. https://doi.org/10.1002/2013JA019440

Liuzzo, L., Feyerabend, M., Simon, S., & Motschmann, U. (2015). The impact of Callisto's atmosphere on its plasma interaction with the Jovian magnetosphere. *Journal of Geophysical Research: Space Physics*, *120*, 9401–9427. https://doi.org/10.1002/2015JA021792

Liuzzo, L., Simon, S., Feyerabend, M., & Motschmann, U. (2016). Disentangling plasma interaction and induction signatures at Callisto: The Galileo C10 flyby. *Journal of Geophysical Research: Space Physics*, *121*, 8677–8694. https://doi.org/10.1002/2016JA023236

Liuzzo, L., Simon, S., Feyerabend, M., & Motschmann, U. (2017). Magnetic signatures of plasmainteraction and induction at Callisto: The Galileo C21, C22, C23, and C30 flybys. *Journal of Geophysical Research: Space Physics*, *122*, 7364–7386. https://doi.org/10.1002/2017JA024303

McComas, D., Allegrini, F., Bagenal, F., Casey, P., Delamere, P., Demkee, D., ... Weidner, S. (2008). The solar wind around Pluto (SWAP) instrument aboard new horizons. *Space Science Reviews*, *140*(1), 261–313. https://doi.org/10.1007/s11214-007-9205-3

McComas, D. J., Elliott, H. A., Weidner, S., Valek, P., Zirnstein, E. J., Bagenal, F., ... Weaver, H. A. (2016). Pluto's interaction with the solar wind. *Journal of Geophysical Research: Space Physics*, *121*, 4232–4246. https://doi.org/10.1002/2016JA022599

Motschmann, U., & Kührt, E. (2006). Interaction of the solar wind with weak obstacles: Hybrid simulations for weakly active comets and for Mars. *Space Science Reviews*, *122*, 197–208. https://doi.org/10.1007/s11,214–006–6218–2

Müller, J., Simon, S., Motschmann, U., Schüle, J., Glassmeier, K., & Pringle, G. J. (2011). A.I.K.E.F.: Adaptive hybrid model for space plasma simulations. *Computer Physics Communications*, *182*(4), 946–966. https://doi.org/10.1016/j.cpc.2010.12.033

Nakai, Y., Shirai, T., Tabata, T., & Ito, R. (1987). Cross sections for charge transfer of hydrogen atoms and ions colliding with gaseous atoms and molecules. *Atomic Data and Nuclear Data Tables*, *37*, 69. https://doi.org/10.1016/0092-640X(87)90005-2

Richards, P. G., Fennelly, J. A., & Torr, D. G. (1994). EUVAC: A solar EUV flux model for aeronomic calculations. *Journal of Geophysical Research*, *99*, 8981–8992. https://doi.org/10.1029/94JA00518

Sauer, K., & Dubinin, E. (2000). The nature of the Martian 'Obstacle Boundary'. *Advances in Space Research*, *26*, 1633–1637. https://doi.org/10.1016/S0273-1177(00)00109-5

Sauer, K., Lipatov, A., Baumgaertel, K., Dubinin, E., & Dubinin, E. (1997). Solar wind-Pluto interaction revised. *Advances in Space Research*, *20*, 295. https://doi.org/10.1016/S0273-1177(97)00551-6

Simon, S., & Motschmann, U. (2009). Titan's induced magnetosphere under non-ideal upstream conditions: 3D multi-species hybrid simulations. *Planetary and Space Science*, *57*(14–15), 2001–2015. https://doi.org/10.1016/j.pss. 2009.08.010

Simon, S., Boesswetter, A., Bagdonat, T., & Motschmann, U. (2007). Physics of the ion composition boundary: A comparative 3D hybrid simulation study of Mars and Titan. *Annales Geophysicae*, *25*(1), 99–115.

Stern, S. A., Bagenal, F., Ennico, K., Gladstone, G. R., Grundy, W. M., McKinnon, W. B., ... Zirnstein, E. (2015). The Pluto system: Initial results from its exploration by New Horizons. *Science*, *350*, AAD1815. https://doi.org/10.1126/science.aad1815

Wahlund, J.-E., Boström, R., Gustafsson, G., Gurnett, D. A., Kurth, W. S., Pedersen, A., ... Mueller-Wordag, I. (2005). Cassini measurements of cold plasma in the ionosphere of Titan. *Science*, *308*(5724), 986–989. https://doi.org/10.1126/science.1109807

Young, L. A., Cook, J. C., Yelle, R. V., & Young, E. F. (2001). Upper limits on gaseous CO at Pluto and triton from high-resolution near-IR spectroscopy. *Icarus*, *153*, 148–156. https://doi.org/10.1006/icar.2001.6662

Young, L. A., Elliot, J. L., Tokunaga, A., de Bergh, C., & Owen, T. (1997). Detection of gaseous methane on Pluto. *Icarus*, *127*, 258–262. https://doi.org/10.1006/icar.1997.5709

Zirnstein, E. J., McComas, D. J., Elliott, H. A., Weidner, S., Valek, P. W., Bagenal, F., ... Young, L. A. (2016). Interplanetary magnetic field sector from Solar Wind around Pluto (SWAP) measurements of heavy ion pickup near Pluto. *Astrophysical Journal*, *823*, L30. https://doi.org/10.3847/2041-8205/823/2/L30